PHYSICAL REVIEW VOLUME 140, NUMBER 1B 11 OCTOBER 1965

# Thorium Resonance Parameters for Neutron Energies from 20 to 222 eV*

E. HADDAD, S. J. FREISENHAHN, F. H. FRÖHNER, AND W. M. LOPEZ
*General Atomic Division of General Dynamics Corporation, John Jay Hopkins Laboratory for Pure and Applied Science, San Diego, California*

(Received 19 April 1965)

The neutron capture cross section for thorium has been measured over the neutron energy region from 20 to 222 eV. The pulsed neutron source for this investigation was obtained by stopping 30-MeV electrons in a water-moderated Fansteel target. The gamma rays resulting from neutron capture were detected by a 4000-liter liquid scintillator. Resonance parameters for the predominant *s*-wave levels were determined from the cross-section data. The resonance parameters were obtained by means of the multisample area-analysis technique. This analysis included multiple-scattering corrections. Of the 11 resonances studied the data indicate that, within the quoted experimental errors, the radiation width remained constant from level to level. The average value obtained for the radiation width was 24.5±1.5 meV.

## I. INTRODUCTION

THE purpose of carrying out neutron-capture research in the resonance region is to obtain information on the properties of nuclear states at excitation energies close to the neutron binding energy. Nuclear quantities that may be obtained from individual levels by capture cross section $[\sigma(n,\gamma)]$ measurements are the resonance energy, level spin, and reaction widths. Information of this type leads to an understanding of the nature of nuclear compound states. In addition, it is useful in the development and checking of nuclear models; it provides the basis for theories on element formation by nucleosynthesis in astrophysics; and it is necessary in reactor design. In this latter field, thorium resonance-parameter data are required to design high-power breeder or converter reactors.

Many transmission measurements have been made which cover the 20- to 222-eV energy region in thorium. In the main, these measurements have produced accurate $\Gamma_n$ data, but the reported values for $\Gamma_\gamma$ have conflicted.[1–3] This paper describes $Th^{232}$ $\sigma(n,\gamma)$ measurements made for the purpose of obtaining more accurate resonance parameters for the predominant *s*-wave resonances occurring between 20 and 222 eV. In particular, the measurements have been directed toward obtaining radiation widths.

Subsequent sections of this paper describe the experimental apparatus used, the experimental measurements made, the analysis techniques used to obtain the resonance parameters, and the experimental results.

## II. EXPERIMENTAL APPARATUS

### A. Target and Collimation System

Bursts of neutrons were obtained by stopping 30-MeV electrons from an *L*-band linear accelerator in a 1.75 in. long water-cooled Fansteel (85% tungsten, 7.5% copper, and 7.5% nickel) target. The spectrum of the primary neutron burst, produced as a result of $(\gamma,n)$ interactions occurring in the target, was shifted into the energy region of interest by means of an aluminum container filled with water. The walls of the aluminum container were 0.030 in. thick. The water moderator defined by the aluminum container was 1 in. thick and 7 in. in diameter. The moderator was placed adjacent to the fansteel target as shown in Fig. 1.

A lead shadow cone was placed along the axis of the neutron beam and between the fansteel target and the capture sample (see Fig. 1). The purpose of the shadow cone was to attenuate the prompt gamma rays originating at the target in order to avoid saturation of the electronics of the scintillation detector during the time of the beam pulse. The shadow cone also served to attenuate the fast neutrons from the primary $(\gamma,n)$ spectrum. After being moderated, the neutrons traveled through an evacuated drift tube and bombarded a sample positioned at the center of a 4000-liter liquid scintillation detector.[4] Collimators placed inside the drift tube reduced the beam diameter from 6 in. at the entrance of the drift tube to 2 in. at the capture sample position. During all measurements the neutron beam intensity was monitored by means of a cadmium covered $BF_3$ chamber placed in the penumbra of the neutron beam.

### B. Detector

The detector used for this investigation was developed to measure neutron-capture cross sections for neutron bombarding energies ranging from 0.01 eV to 30 keV. (Details of the detector may be found in Ref. 4.) It was designed to have an intrinsic efficiency[5] $(\epsilon_i)$ of 80% for a single 8-MeV gamma ray originating at the center of the detector. This results in a detection efficiency which is essentially independent of gamma-ray cascade mode.

---

* This work was supported in part by the United States Atomic Energy Commission under Contract AT(04-3)-167.

[1] D. J. Hughes, B. A. Magurno, and M. K. Brussel, Brookhaven National Laboratory Report BNL-325, Suppl. 1, 2nd ed., 1960 (unpublished).

[2] C. A. Utley and R. H. Jones, in United Kingdom Atomic Energy Agency Report AERE-PR/NP-2 (unpublished).

[3] J. B. Garg, J. Rainwater, J. S. Petersen, and W. W. Havens Jr., Phys. Rev. 134, B985 (1964).

[4] E. Haddad, R. B. Walton, S. J. Friesenhahn, and W. M. Lopez, Nucl. Instr. Methods 31, 125 (1964).

[5] The intrinsic efficiency is the probability for a gamma ray to have at least one interaction in the scintillator solution before escaping from the detector.

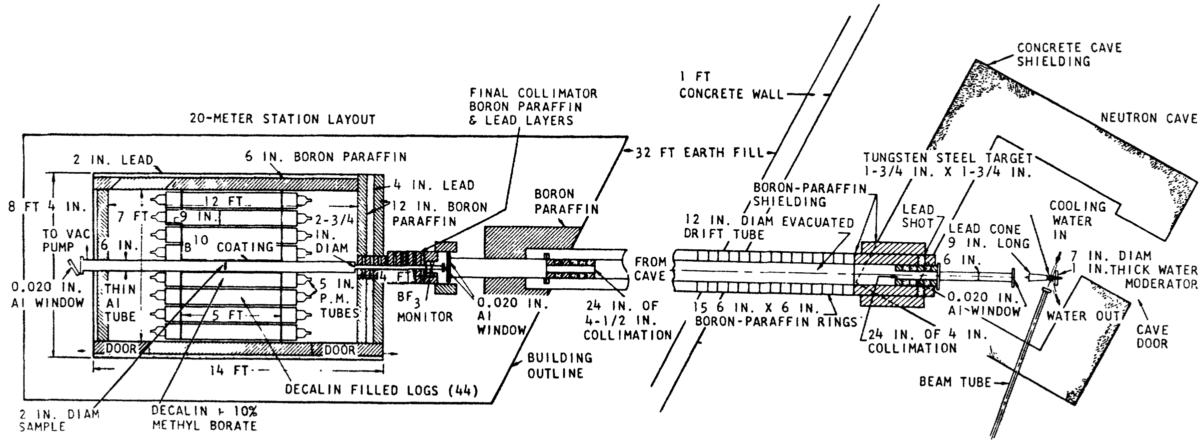

FIG. 1. Experimental arrangement of target, detector, and collimation system used for $\sigma(n,\gamma)$ measurements.

The equation for the over-all detection efficiency is $\epsilon_\gamma = \epsilon_i \epsilon_b$, where $\epsilon_b$ is the experimentally determined spectrum fraction (fraction of the area under a gamma-ray pulse-height distribution above a given bias). For thorium, in which the total energy emitted is 5.3 MeV,[6] $\epsilon_i$ is taken to be $(97 \pm 3)\%$.[4]

The detector (see Fig. 1) consists of a 2-ft diam, hollow central Plexiglas annulus surrounded by an array of forty-four 9-in. diam, hollow Plexiglas cylinders (logs). Each end of an individual log is viewed by a 5-in. photomultiplier tube (CBS-7819 or Dumont 6364). To reduce light losses, the areas at the ends of each log not covered by the photomultiplier were painted with white Tygon paint. Each end of the central annulus is viewed by eight 5-in. photomultiplier tubes. The samples for the thorium measurements were placed in an evacuated 6.0-in.-diam aluminum liner positioned inside and concentric to a 6.5-in.-diam hole that extends through the central annulus. Wrapped around the aluminum liner was a 0.125-in.-thick $B^{10}$ epoxy sheet. The collimated neutron beam enters the detector through a 0.020-in. aluminum window, then passes into the evacuated liner. The liquid scintillator solution used in the logs is decahydronaphthalene (decalin) containing 1 g/liter of *p*-terphenyl, 2 g/liter of 2,5 diphenyloxazole (PPO), and 0.05 g/liter of dimethyl *p*-bis[2-(5-phenyloxazoyl)]-benzene (dimethyl POPOP). The scintillator solution used in the 2-ft central annulus was the same as that used in the logs with one exception: it also contained trimethyl borate (10% by volume). The trimethyl borate was added to the solution in the central annulus to suppress the 2.2-MeV gamma rays resulting from in-scattered neutrons being captured by hydrogen.

### C. Electronics

A block diagram of the electronic system used for the measurements is shown in Fig. 2. The anodes of the 52 photomultiplier tubes at one end of the detector are connected in parallel with unshielded conductors and constitute a tube bank. The total capacitance of the anode network of each bank is ~500 pF, which is considerably smaller than would be obtained using coaxial cable. Two distribution panels, one for each bank, were used to supply separate high voltages to the individual tubes. The gains of the log-tube combinations were matched to within a few percent of each other by using a radioactive source at a standard position with respect to each log. To reduce the accelerator-induced noise pickup to an acceptable amount, the entire system was enclosed with fine-mesh copper screen grounded to the outer shield of the triaxial cable that connects the 20-meter station (detector) and the data gathering station.

A timing signal from the linear accelerator, which is coincident with the burst of electrons striking the neutron target, triggers a crystal-controlled digital delay generator. After a preset time, this delay generator starts a multichannel time analyzer and also triggers a time-gate generator. The gamma rays resulting from neutron captures in thorium interact with the scintillator solution, which in turn produces a pulse from each tube bank. The simultaneous signals from the two banks of photomultiplier tubes are amplified and inverted by two preamplifiers that drive the signals through ~200 ft of triaxial cable. The signals are further amplified by two A-8 amplifiers,[7] which are part of the fast-coincidence system between the two banks of photomultiplier tubes. This fast-coincidence system is used to eliminate spurious photocathode noise pulses. The signals from the preamplifiers are also fed to a summing amplifier that algebraically adds the amplitudes of the

---

[6] L. V. Groshev, A. M. Demidov, J. N. Lutsendo, and J. I. Pelekhov, *Atlas of X-Ray Spectra from Radiative Capture of Thermal Neutrons* (Pergamon Press, Ltd., London, 1959).

[7] G. G. Kelley, IRE Natl. Conv. Record, **9**, 63 (1957).

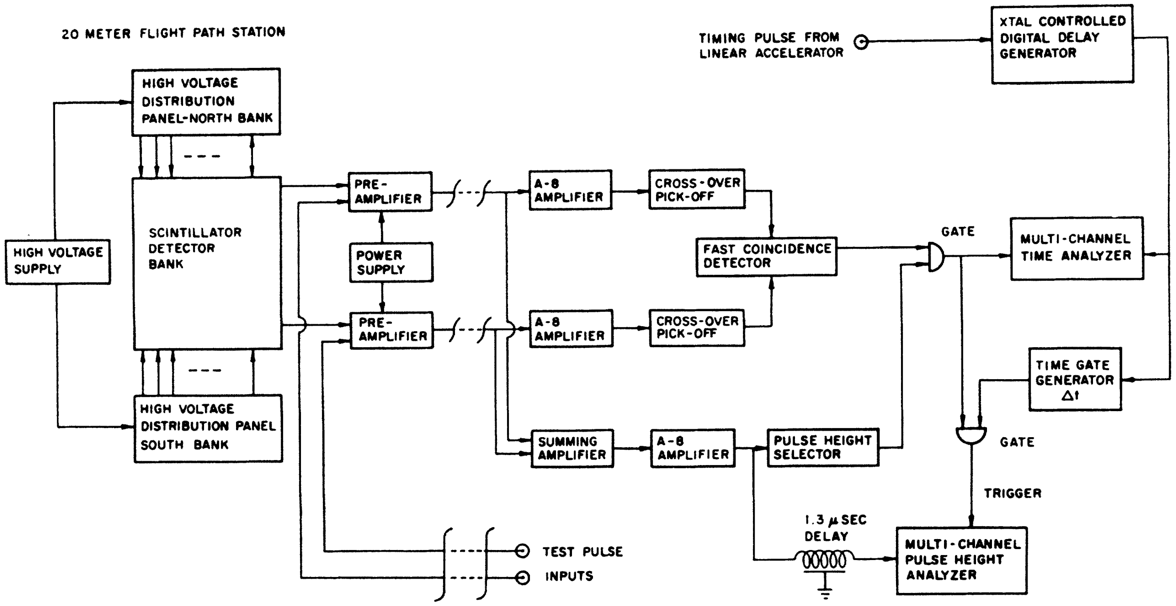

FIG. 2. Block diagram of liquid-scintillator electronics system.

two signals. The sum is then proportional to the total energy deposited in the detector system by the capture gamma rays.

The outputs of the A-8 amplifiers in the coincidence channels are analyzed by tunnel diode[8] "crossover pick-off" units. These units generate a pulse that is related in time to the instant the symmetrical output pulse from the A-8 amplifier crosses the zero axis. This point in time is relatively independent of the pulse amplitude and allows fast coincidence detection between both signals. The timing pulses from the crossover pick-off circuits are fed to a tunnel diode coincidence detector having a 0.25-μsec resolving time. The output pulse of the fast coincidence detector is passed through a gate (normally closed) if it is in slow coincidence with the summed pulse accepted by the pulse-height selector. This pulse-height selector has the characteristic that the upper and lower limits of the window are independently adjustable. The upper threshold is set so that large overload sum pulses, which are of cosmic-ray origin, are rejected. The lower threshold is set to accept pulses corresponding to the capture gamma rays from thorium but to discriminate against unwanted backgrounds.

The gated coincidence pulses are stored in a TMC 1024-channel time analyzer which gives a time history of the gamma rays resulting from radiative capture in the thorium sample. The coincidence pulses also trigger a multichannel pulse-height analyzer, which serves two purposes. First, it is used to set the upper and lower thresholds of the pulse-height selector at the energy levels desired. This is done prior to the thorium data runs with radioisotopes having known gamma-ray energies. For the thorium measurements the lower threshold was set at 4.0 MeV and the upper threshold was set at 10.0 MeV. Second, the analyzer was used to obtain gamma-ray pulse-height distributions associated with a particular resonance. The neutron energy interval was selected by a combination of the crystal-controlled digital delay and the time gate generators.

The time resolution of the detector and its associated electronics was determined to have a full width at half-maximum intensity of 28 nsec.[8]

The dead time of the electronics, not including the multichannel analyzer, is 2 μsec, and the analyzer dead time is 16 μsec. Consequently, the data are corrected for these counting losses.

## III. EXPERIMENTAL PROCEDURES

### A. General Discussion

When a neutron is captured by a nucleus in the sample, the excitation energy is given off in the form of prompt gamma rays, nearly all of which are absorbed within the 4000-liter liquid scintillator, which in turn results in an output pulse from the detector. The time histories of the capture pulses are recorded on a multichannel time analyzer, and the energy of the neutrons captured in the sample may be obtained from the flight time and known neutron flight-path distance. The instantaneous counting rate, for a single burst from the accelerator (corrected for backgrounds), expected in channel $i$ of the analyzer between $t$ and $t+\Delta t$ is given by

$$\Delta C_i/\Delta t \cong c_i = S\phi(t) f(E,n)\epsilon_\gamma(E)\,, \qquad (1)$$

where $\phi(t)$ is the neutron flux incident on the sample

---

[8] E. Haddad, S. J. Friesenhahn, and W. M. Lopez, U. S. Atomic Energy Commission Report GA-3874, General Atomic, 1963 (unpublished).

between $t$ and $t+\Delta t$, $S$ is the sample area normal to the beam, $f(E,n)$ is the probability that a neutron of energy $E$ is captured in the sample, $n$ is the sample thickness in nuclei per square centimeter, $\epsilon_\gamma(E)$ is the detector efficiency, and $\Delta t$ is the channel width. In Eq. (1) the flux has the units of neutrons cm$^{-2}$ sec$^{-1}$.

In this work the parameters of a resonance are obtained by an analysis of the capture area $C$ defined as

$$C(n,E_1,E_2)=\sum_{i=i_1}^{i_2}\Delta C_i$$

$$=S\int_{E_1}^{E_2}dE\,\phi(t)\frac{dt}{dE}f(E,n)\epsilon_\gamma(E)\,, \quad (2)$$

where $E_1$ and $E_2$ define an energy interval containing the resonance, and $i_1$ and $i_2$ are the channel numbers corresponding to $E_1$ and $E_2$, respectively. If resolution effects cannot be neglected, the following equation is used:

$$\bar{C}(n,E_1,E_2)=S\int_{E_1}^{E_2}dE$$

$$\times\int_0^\infty dE'r(E,E')\phi(t')\frac{dt'}{dE'}f(E',n)\epsilon_\gamma(E')\,. \quad (3)$$

Here $r(E,E')dE$ is the probability (normalized to unity) that a capture event due to a neutron with energy $E'$ is actually recorded in time as if the energy had been between $E$ and $E+dE$. In using the area analysis technique for well separated levels, the effect of instrumental resolution may be neglected by choosing the energy boundaries far out in the wings of the resonance.

It is convenient to separate the probability of capture, $f(E,n)$, into two parts—a part giving the probability of capture on the first interaction, $f_0(E,n)$, and a part giving the probability of capture after one or more scatterings, $f_s(E,n)$.[9] For convenience $f(E,n)$ is written as $f$. The capture probability, $f$, can then be written as

$$f=f_0+f_s \quad (4)$$

or as

$$f=(\bar{\sigma}_\gamma/\bar{\sigma})[1-\exp(-n\bar{\sigma})]+f_s\,, \quad (5)$$

where $\bar{\sigma}_\gamma$ is the Doppler-broadened capture cross section and $\bar{\sigma}$ is the Doppler-broadened total cross section. The term $f_s$ is called the multiple-scattering term.

Since the thorium resonances considered here are well isolated and only neutron energies of less than 222 eV are considered, the cross sections are well represented as sums of Doppler-broadened single-level Breit-Wigner terms ($s$-wave interactions only). The expressions which were used in the cross sections appearing in Eq. (5) are given by

$$\bar{\sigma}_\gamma=\sum_\lambda\bar{\sigma}_{\gamma,\lambda}\,;\quad \bar{\sigma}_n=\sigma_p+\sum_\lambda\bar{\sigma}_{n,\lambda}\,;\quad \bar{\sigma}=\bar{\sigma}_\gamma+\bar{\sigma}_n\,, \quad (6)$$

where the subscript $\lambda$ denotes a particular level and where

$$\bar{\sigma}_{\gamma,\lambda}=[\sigma_0(\Gamma_\gamma/\Gamma)(E_0/E)^{1/2}\psi(x,\beta)]_\lambda \quad (7)$$

is the neutron-capture cross section and

$$\bar{\sigma}_{n,\lambda}=[\sigma_0(\Gamma_n/\Gamma)\psi(x,\beta)+(2R/\bar{\lambda}_0\alpha)\phi(x,\beta)]_\lambda \quad (8)$$

is the neutron elastic-scattering cross section. In these equations conventional notation is used.[1,10] We describe below how the quantities $\epsilon_\gamma(E)$ and $\phi(E)$ were determined experimentally.

### B. Relative Flux Measurement

To obtain resonance parameters with the area analysis technique, the quantity $S\epsilon_\gamma\phi(t)$ appearing in Eq. (2) must be determined. This was done as follows.

The flight-time dependence of the neutron flux incident on the capture sample was measured over the energy range 1 eV to 1 keV by placing a low-pressure 2-in.-diam BF$_3$ counter[11] behind the liquid scintillator at the exit point of the collimated neutron beam. This position is $(21.20\pm0.03)$ meters from the neutron source. A $1/v$ detection efficiency was assumed for the BF$_3$ counter over the entire energy range of interest.[12] If $c(t)$ is the observed counting rate from the BF$_3$ counter as a function of flight time, then $c(t)[E(t)]^{1/2}$ is proportional to the neutron flux $\phi(t)$, where $E(t)$ is the energy corresponding to the flight time $t$. Figure 3 is a plot of $\log\{c(t)[E(t)]^{1/2}\}$ versus $\log E(t)$ derived from the BF$_3$ counter data. The linear behavior of the log-log plot implies that $\phi(t)$ may be described by

$$\phi(t)=K[E(t)]^\alpha\,, \quad (9)$$

where the exponent $\alpha$ is found from the slope of the curve shown in Fig. 3, and $K$ is a constant that determines the absolute flux $\phi(t)$. Using Eq. (9) and $dt/dE=L(mE^{-3}/8)^{1/2}$, and assuming that $\epsilon_\gamma$ is constant over the neutron energy interval containing the resonance, we can rewrite Eq. (2) as

$$C(n,E_1,E_2)=\epsilon_\gamma SKL(m/8)^{1/2}\int_{E_1}^{E_2}dE\,E^{\alpha-3/2}f(E,n)\,, \quad (10)$$

where $L$ is the flight path and $m$ is the neutron mass.

To obtain resonance parameters from Eq. (10) the quantity $\epsilon_\gamma SK$ must be measured. This was done for thorium by using the "saturated resonance" technique. This technique consists of using a sample thick enough

---

[9] F. H. Fröhner, D. L. Huffman, E. Haddad, and W. M. Lopez, General Atomic Report GA-5816, 1965 (unpublished).

[10] F. H. Fröhner and E. Haddad, Nucl. Phys. (to be published).

[11] Purchased from 20th Century Electronics, Ltd., London, Type No. 41EB70/50G.

[12] H. Bischel and T. W. Bonner, Phys. Rev. **108**, 1025 (1957).

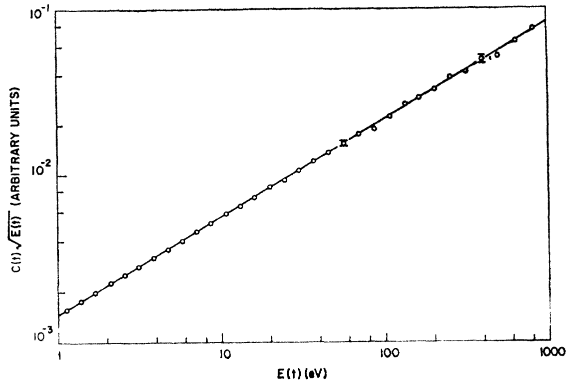

FIG. 3. Experimental curve of data obtained with a BF$_3$ counter as a function of energy, measured at exit point of collimated beam. Data are corrected for $1/v$ response of BF$_3$ counter.

that the transmission is nearly zero in the peak region of some low-energy ($E_0\leq 100$ eV) resonance where capture predominates over elastic scattering. In this case $\Gamma_\gamma\gg\Gamma_n$ and $n\bar{\sigma}(E_0)\gg 1$; thus, Eqs. (1) and (9) yield

$$(\Delta C/\Delta t)|_{E_0}=\epsilon_\gamma SKE_0^\alpha f(E_0) \tag{11}$$

for the counting rate in channel $i$ at the peak of the saturated resonance.

With Eqs. (5), (7), and (8), and neglecting potential scattering and the contributions from other resonances, we get

$$f(E_0)\approx(\Gamma_\gamma/\Gamma)+f_s(E_0). \tag{12}$$

Solving Eq. (11) for $\epsilon_\gamma SK$ we write

$$\epsilon_\gamma SK\approx(E_0^\alpha[(\Gamma_\gamma/\Gamma)+f_s(E_0)])^{-1}(\Delta C_i/\Delta t)|_{E_0}. \tag{13}$$

Figure 4 shows some typical time-of-flight data for the levels at 21.8 and 23.5 eV, obtained with a 0.05-in.-thick thorium sample. From this type of data the quantities $E_0$ and $\Delta C_i/\Delta t$ are obtained for use in Eq. (13).

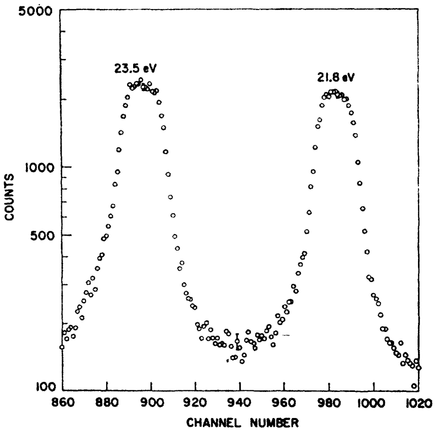

FIG. 4. Typical time-of-flight data for 21.8- and 23.5-eV levels in thorium obtained with thick samples ($n=3.83\times10^{-3}$ nuclei/b), 0.125-$\mu$sec time channel width, and 0.1-$\mu$sec accelerator burst width.

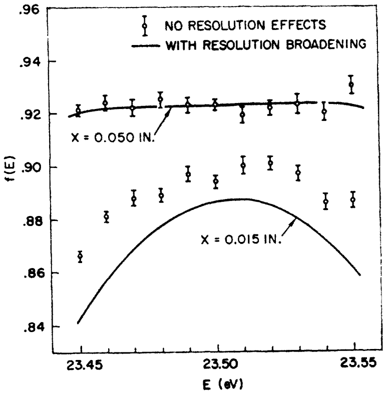

FIG. 5. Diagram showing calculated effects of instrumental resolution broadening in vicinity of peak of 23.5-eV level in thorium, for two sample thicknesses. Ordinate $f(E)$ is probability of capture for incident neutron. The error bars indicate the uncertainty in the Monte Carlo calculation.

Since the saturated resonance technique requires that counts in the peak of the resonance be used in determining $\epsilon_\gamma SK$, neglecting potential scattering and instrumental resolution effects may introduce some error into Eq. (13). In order to determine the magnitude of these effects, a computer calculation of $f(E_0)$ was made which included the effects of potential scattering, contributions from neighboring resonances, and instrumental resolution effects. In this calculation $f(E)$ was convoluted with a Gaussian resolution function:

$$\langle f(E_0)\rangle\approx\frac{1}{R(E_0)\pi}\int_{-\infty}^{\infty}f(E)\exp\left[-\frac{(E_0-E)^2}{R(E_0)^2}\right]dE. \tag{14}$$

The resolution width was taken as

$$R(E_0)=2E_0[(t_c^2+t_b^2+12t_j^2)(E_0/3mL^2)+2(\delta L/L)^2]^{1/2}, \tag{15}$$

where $t_c$ = time-analyzer channel width, $t_b$ = accelerator burst width, $t_j$ = timing jitter of the detector-electronic system, and $\delta L$ = effective-flight-path uncertainty re-

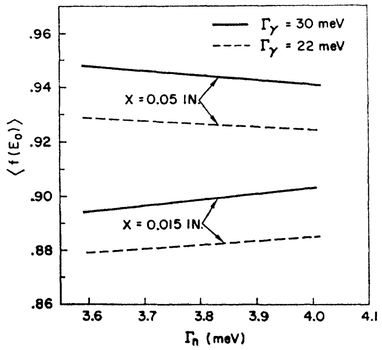

FIG. 6. Calculated curves of $\langle f(E_0)\rangle$ for 23.5-eV resonance in thorium as a function of $\Gamma_n$ for two assumed values of $\Gamma_\gamma$ and two sample thicknesses. Curves show that calculated probability of neutron capture in peak of "saturated resonance" is not very sensitive to assumed parameters.

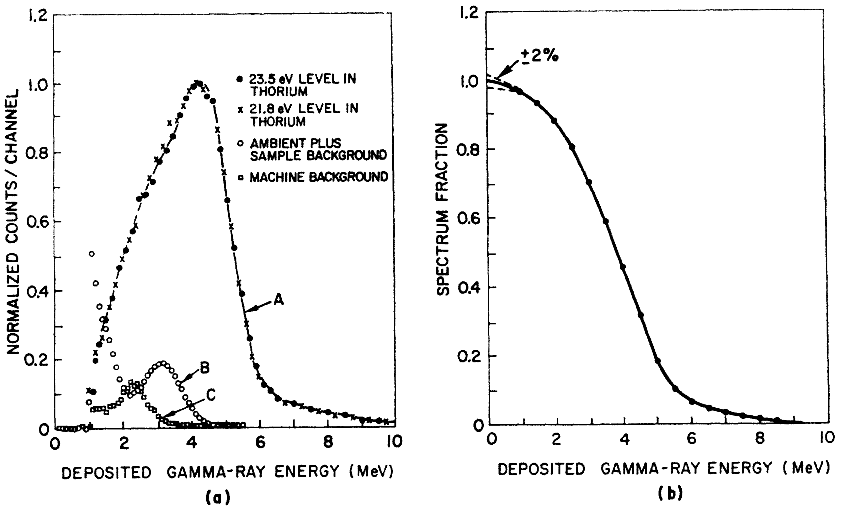

FIG. 7. (a) Comparison of pulse-height distributions from 4000-liter liquid scintillator resulting from neutron captures in 21.8- and 23.5-eV resonances of thorium. Curve A has been corrected for background contributions, shown as curves B (ambient) and C (machine). Data were taken with 0.050-in. samples ($n=3.83\times10^{-3}$ nuclei/barn) and a 1-MeV electronic bias. (b) Normalized integral curve derived from curve A of Fig. 7(a), showing spectrum fraction $E_b$ as a function of electronic bias (which is given here in terms of photon energy deposited in scintillator).

flecting the moderator effects on the fast-neutron pulse. For a derivation of this resolution-broadening equation see Ref. 10. Figure 5 shows the computer-calculated curves of $f(E)$, with and without the resolution broadening of Eq. (14), in the neighborhood of $E_0=23.5$ eV. From these curves we see virtually no resolution effects at $E_0$ for the thick sample (0.050 in.) and only a small effect for the thinner sample (0.015 in.). These small resolution effects on $\epsilon_\gamma SK$ may be corrected for in Eq. (13) by substituting the computer-calculated value of $\langle f(E_0)\rangle$ for $[\Gamma_\gamma/\Gamma+f_s(E_0)]$. However, whether the exact or approximate value of $f(E_0)$ is used, the solution of Eq. (13) for $\epsilon_\gamma SK$ requires $\Gamma_\gamma$ and $\Gamma_n$, which one does not usually know *a priori*. Figure 6 shows computer-calculated curves of $\langle f(E_0)\rangle$ for the 23.5-eV level as a function of assumed values for $\Gamma_n$ and $\Gamma_\gamma$ in the expected range of these parameters. From the figure it is seen that $\langle f(E_0)\rangle$ is relatively insensitive to small changes in $\Gamma_n$ or $\Gamma_\gamma$.

To determine the "best value" of $\epsilon_\gamma SK$ requires that the "best values" of $\Gamma_\gamma$ and $\Gamma_n$ be used. Consequently, an iterative procedure was used to obtain $\epsilon_\gamma SK$ in which the parameters for Eq. (13) are obtained by the method described in Sec. IV. This iterative procedure was used with the 21.8-eV level and independently with the 23.5-eV level. This resulted in two values of $\epsilon_\gamma SK$ for each thick-sample data run. The statistical accuracy of each $\epsilon_\gamma SK$ determination was of the order of 3%, and the agreement between each pair of values obtained with a given data run was consistent within this accuracy. However, the values of $\epsilon_\gamma SK$ obtained from the 23.5-eV level were consistently higher than those obtained from the 21.8-eV level. The ratio

$$R=\epsilon_\gamma SK(23.5\text{ eV})/\epsilon_\gamma SK(21.8\text{ eV}),$$

which was obtained from averaging nine data runs over a period of 4 months, gave an $\bar{R}$ of 1.03±0.005.

This systematic difference in the $\epsilon_\gamma SK$ values obtained from the 21.8- and 23.5-eV levels in $\mathrm{Th}^{232}$ could be due to inaccuracies in the $f(E_0)$ calculations, since the quantity $f(E_0)$ for a given level is common to all $\epsilon_\gamma SK$ determinations with that level. It is estimated that $f(21.8\text{ eV})$ and $f(23.5\text{ eV})$ determined by the iterative procedure with $\Gamma_\gamma$, $\Gamma_n$ contain an uncertainty of 2% to 3%.

The systematic $\epsilon_\gamma SK$ difference could also be due to level dependence on the detection efficiency $\epsilon_\gamma$. This could only result from a drastic difference in the gamma-ray spectra seen by the large liquid scintillator, resulting, for example, from a high probability for ground-state transitions in one level and not in the other. This is considered very unlikely for the $s$-wave levels in thorium, since all the level spins are the same.[13] Furthermore, if such were the case, one would expect to see some differences in the pulse-height distributions observed from these two levels. Figure 7 shows two such overlapped pulse-height distributions. With an electronic bias of 4 MeV for taking time-of-flight data, we see from Fig. 7 at most a difference of 2%. Consequently, the systematic 3% difference in the $\epsilon_\gamma SK$ determination is most likely due to inaccuracies in the $f(E_0)$ calculations.

In the analysis of the eleven $s$-wave levels an average value of $\epsilon_\gamma SK$ was determined for each data run from the 21.8- and 23.5-eV resonances. The uncertainty assigned to $\epsilon_\gamma SK$ was ±3%.

### C. Pulse-Height Distributions

In order to assign some confidence limits to the assumption that the detection efficiency does not change over the neutron energy interval from 20 to 222 eV (which includes the 11 $s$-wave levels under investiga-

---

[13] J. B. Marion and J. L. Fowler, *Fast Neutron Physics* (Interscience Publishers, Inc., New York, 1963), Vol. II, p. 1751.

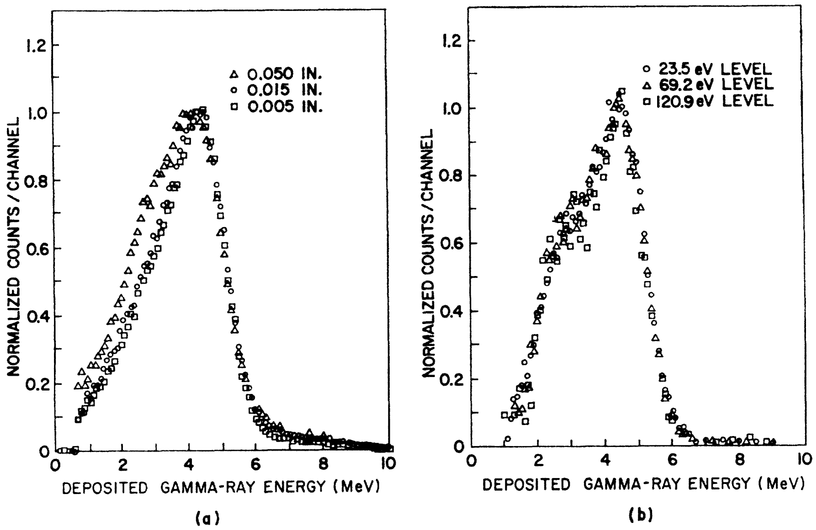

FIG. 8. (a) Comparison of pulse-height distributions resulting from neutron capture in thorium samples of various thicknesses. (b) Comparison of pulse-height distributions resulting from neutron capture in three different resonances.

tion), pulse-height distributions for many of the thorium levels were measured and compared.

The background-corrected curve for the 23.5-eV level (see left-hand side of Fig. 7) was obtained from four separate pulse-height distribution measurements. The four measurements were (1) ambient background—neutron beam off, sample out; (2) sample background—neutron beam off, sample in; (3) machine background—neutron beam on, sample out; (4) capture data—neutron beam on, sample in. These data were taken during a gated time interval of 6 μsec appropriately delayed from the neutron burst (see block diagram of Fig. 2). The curves in Fig. 7 are all relative to curve A, which is normalized to unity at the peak of the distribution. Curve B in Fig. 7 results from the natural radioactivity of the thorium sample plus the ambient background. Curve C results from neutron captures with no sample in the beam and represents a form of background that is time dependent and proportional to the neutron beam intensity (backgrounds are described further in a later section). It can be seen from the data in Fig. 7 that the extrapolation to zero pulse height of curve A is sensitive to the errors in the background subtractions. From a study of many pulse-height distributions of the same level taken under various experimental conditions, such as different counting rates, time intervals, and backgrounds, an uncertainty of ±3% is assigned to a spectrum fraction ($\epsilon_b$) determination. Spectrum fractions obtained from the 21.8, 23.5, 69.2, and 120.9-eV levels (see Figs. 7 and 8) agree with each other within the accuracy of the measurements. Consequently, we assign an uncertainty of ±3% to the assumption that the detection efficiency $\epsilon_\gamma$ is constant.

### D. Gamma-Ray Attenuation in Sample

Another factor that requires evaluation is the effect of sample thickness on the detection efficiency $\epsilon_\gamma$, since in the present case physically thick samples must be used with the "saturated resonance" technique to determine the quantity $\epsilon_\gamma SK$. The left-hand side of Fig. 8 shows three pulse-height distributions (normalized to unity at the peak) of the 23.5-eV level obtained with three sample thicknesses—0.050 in., 0.015 in., and 0.005 in. As seen from Fig. 8, the total gamma-ray energy observed from a thick sample is degraded by energy losses in the sample. For a given bias level $E_b$ this results in a smaller spectrum fraction $\epsilon_b$ for thick samples. One can postulate an exponential behavior of the spectrum fraction as a function of sample thickness $x$ as

$$\epsilon_b(x,E_b)=\epsilon_b(0,E_b)e^{-kx}. \qquad (16)$$

This behavior of $\epsilon_b$ is at least qualitatively consistent with data such as those shown in Fig. 8. A direct measure of this effect is the ratio of $\epsilon_\gamma SK$ values obtained with samples 0.015 in. and 0.050 in. thick (as described in Sec. IIIB). The ratio

$$\epsilon_\gamma SK(0.015\ \text{in.})/\epsilon_\gamma SK(0.050\ \text{in.})=1.10\pm0.02$$

was obtained with data from the 21.8-eV and 23.5-eV levels in thorium using a 4-MeV bias. From this ratio, the exponent $k$ in Eq. 16 is $(2.7\pm0.5)$ in.$^{-1}$. This results in a correction of approximately (3±0.5)% to $\epsilon_\gamma SK$ in going from a 0.015-in.-thick sample to a 0.005-in.-thick samples. The correction for a 0.0005-in.-thick sample was (4±0.5)%.

### E. Backgrounds

Three types of backgrounds (see Fig. 9) are present for a time-of-flight capture measurement when the sample is positioned in the neutron beam: (1) ambient, (2) machine associated, and (3) neutrons scattered by the sample. To reduce the effects from (1) and (2), borated paraffin and lead shielding are placed around

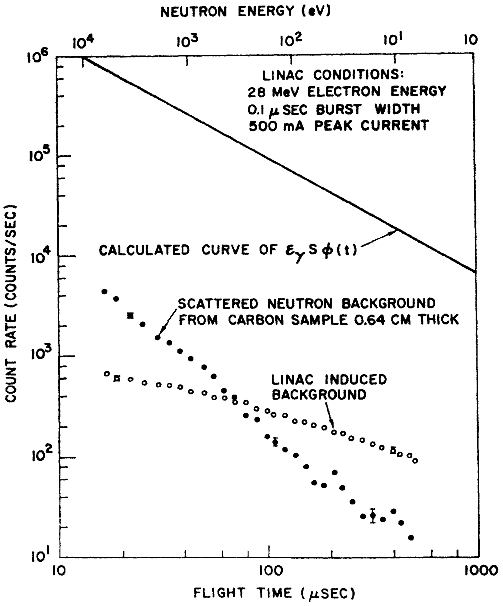

FIG. 9. Time-dependent backgrounds relative to counting rate with a hypothetical thorium sample that captures all incident neutron flux ($\epsilon_\gamma SKE^\alpha$).

the detector. Details of the shielding arrangement are described in Ref. 4.

The ambient background arises primarily from cosmic-ray interactions within the detector and from the natural radioactivity present in the detector and its environment. With thorium samples, there is an additional constant gamma-ray background from the natural radioactivity in the samples. The gamma-ray energy distribution of the ambient and sample backgrounds is shown in Fig. 7. As seen from this figure, the gamma-ray background from the thorium sample has an energy distribution that peaks at ~3.1 MeV. Consequently, in order to optimize the signal-to-background ratio, a 4-MeV lower bias and a 10-MeV upper bias were used when time-of-flight capture data were taken. Table I lists the ambient-background counting rates that were present with the three thickest thorium samples.

The time-dependent machine background is that background above ambient which is observed with the accelerator on and no sample in the neutron beam. Its magnitude depends on the intensity of the neutron beam and its time dependence is characteristic of the time dependence of the neutron flux. This background is thought to be caused by neutrons scattered and captured in the vicinity of the collimator placed just in front of the detector. The gamma-ray energy distribution of this background is shown in Fig. 7 and is due primarily to neutron captures by hydrogen in the detector environment.

TABLE I. Background counting rates from thorium samples with the detector threshold set at 4 MeV.

| Sample thickness (in.) | Background (counts/sec) |
|---|---|
| No sample | 115 |
| 0.005 | 175 |
| 0.015 | 300 |
| 0.050 | 640 |

The scattered-neutron background is the result of neutrons which undergo potential or resonant elastic scattering within the sample and are subsequently captured in the detector materials. The neutrons which undergo scattering and escape from the sample may be captured in the 0.083-in.-thick aluminum liner or the 0.125-in.-thick $B^{10}$ epoxy linear that surrounds the aluminum liner. The neutrons may also enter the liquid-scintillator volume, where they will be captured in boron, hydrogen, or carbon, in that order of probability.

If multiple scattering is neglected, the enhancement of the observed capture area $C_{\text{obs}}$ over the area $C$ of Eq. (2) due to resonance-scattered neutrons is approximately given by[14]

$$C_{\text{obs}}(n,E_1,E_2)=C(n,E_1,E_2)(1+\epsilon_n\Gamma_n/\epsilon_\gamma\Gamma_\gamma)\,, \quad (17)$$

where $\epsilon_n$ is the efficiency for the detection of neutrons scattered into the detector. The ratio $\epsilon_n:\epsilon_\gamma$ was obtained as follows: First the product $\phi\epsilon_\gamma$ (flux times efficiency) was determined by the "saturated resonance" technique described in Sec. IIIB, using the 23.5-eV level of thorium. The thorium sample was then replaced by a pure scatterer (carbon). From the counting rates recorded with the two samples $\epsilon_n:\epsilon_\gamma$ was calculated for various energies. The result is shown in Fig. 10.

For the 69.2-eV resonance, Eq. (17) gives a correction of about 0.6%. Actually this is an upper limit, because so far we have neglected the time delay between the scattering of the neutron and its capture in the detector. The mean life of a scattered 69.2-eV neutron in the detector was estimated as ~11 μsec, whereas the interval $(E_1,E_2)$ of the area analysis corresponds to ~3.8 μsec. Thus resonance-scattered neutrons con-

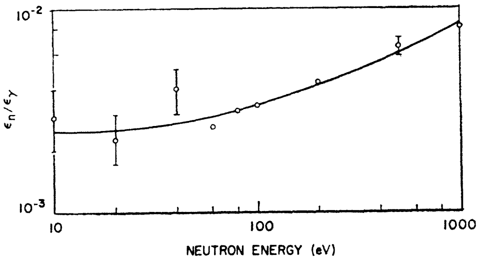

FIG. 10. Ratio of detection efficiency for scattered neutrons ($\epsilon_n$) to detection efficiency for radiative capture ($\epsilon_\gamma$) in thorium as a function of neutron energy.

---

[14] D. Zeliger, N. Iliescu, Kim Hi San, D. Longo, L. B. Pikel'ner, É. I. Sharapov, Zh. Eksperim. i Teor. Fiz. **45**, 1294 (1963) [English transl.: Soviet Phys.—JETP **18**, 889 (1964)].

tribute much less to the counting rate in the range $(E_1,E_2)$ than given by Eq. (17). Furthermore the data did not show any evidence of the broad "bump" on the low-energy side of strong resonances expected due to delayed capture of the resonance-scattered neutrons. Thus the effect seems to be very small and no correction was made.

A correction for potential scattering of neutrons was applied to the thorium data using the results of the carbon scattering run and the ratio of the potential scattering cross sections of carbon and thorium. In all cases this correction was less than 0.6%.

Neutron induced fission can occur in thorium for neutron energies $\geq 1$ MeV. The resulting fission products could result in a time-dependent gamma-ray background. However, the 9-in. lead cone placed between the pulsed neutron source and the capture sample effectively attenuates the primary neutrons by a factor of 50. Furthermore, an examination of the data in the region between resonances did not reveal any evidence of an extraneous background.

## IV. METHOD OF ANALYSIS

The partial widths of the thorium resonances were obtained using a multithickness area analysis FORTRAN-IV code (GACA) written for an IBM 7044.[9] The analysis is based on Eq. (10), which relates the number of counts under a peak to the resonance parameters and the sample thickness, $n$. The relationship is

$$C(n,E_1,E_2)=C(\Gamma_n,\Gamma_\gamma,n)$$

$$=\epsilon_\gamma SKL(m/8)^{1/2}\int_{E_1}^{E_2} dE\, E^{\alpha-3/2}f(E,n).$$

The various quantities appearing in this equation have already been defined in Sec. IIIB. The capture area is also a function of the statistical spin factor $g$ and the resonance energy, $E_0$. For thorium, which is an even-even nucleus, we are only concerned with $C(\Gamma_n,\Gamma_\gamma,n)$ since $g=1$ and $E_0$ is sufficiently well known from the position of the resonance peaks.

In the code GACA the expression $C(\Gamma_n,\Gamma_\gamma,n)$ is equated to the observed capture areas:

$$C(\Gamma_n,\Gamma_\gamma,n)=C_{\text{obs}}=\sum_{i=i_1}^{i=i_2}\Delta C_i, \tag{18}$$

and this equation is solved for $\Gamma_n$ at a series of fixed $\Gamma_\gamma$ values (or vice versa). Thus, for a given thickness $n$, the curve $\Gamma_n$ versus $\Gamma_\gamma$ represented by Eq. (18) is generated. Equation (18) is solved by a modified Newton-Raphson method. If $\Gamma_n^{(0)}$ is a first guess, then Newton's formula for the improved value $\Gamma_n^{(1)}$ is

$$\Gamma_n^{(1)}=\Gamma_n^{(0)}-(C-C_{\text{obs}})/(\partial C/\partial\Gamma_n^{(0)}). \tag{19}$$

Now $C$ can be written as the sum

$$C=C_0+C_s, \tag{20}$$

where $C_0$ describes capture in the first interaction and $C_s$ describes capture after one or more scattering collisions in the sample. Since $C_s$, or rather $f_s$ (see Ref. 9), is calculated by means of the Monte Carlo technique, its derivative cannot be readily obtained. Therefore, Eq. (19) was replaced by

$$\Gamma_n^{(1)}=\Gamma_n^{(0)}-(C_0+C_s-C_{\text{obs}})/(\partial C_0/\partial\Gamma_n^{(0)}), \tag{21}$$

which means that the $\Gamma_n$ dependence of $C_s$ is neglected. It turned out that this did not affect the convergence of the process appreciably. The improved quantity $\Gamma_n^{(1)}$ is then used as the initial value for the next step in the iteration. The code iterates until the criterion

$$(C-C_{\text{obs}})/C_{\text{obs}}\leq \max(\epsilon,\delta C_s/C) \tag{22}$$

is fulfilled, where $\epsilon$ is a small preset number and $\delta C_s/C$ is the relative statistical uncertainty in $C$ due to the Monte Carlo character of the $f_s$ calculation.

For well isolated resonances the limits $E_1,E_2$ of $C$ can be taken far out in the wings, so that resolution effects are negligible. In these cases $C$ was not resolution broadened.

Two assumptions were made to simplify the calculation of $f_s$: multiple scattering was treated as if (1) the target nuclei were at rest and initially had Doppler-broadened cross sections (this is correct for $f_0$ but only an approximation for $f_s$) and (2) scattering was isotropic in the laboratory system (which would be correct for infinitely heavy target nuclei).

Checks were made against a code[15] which treats multiple scattering rigorously, and the results are given in Fig. 11. The figure shows that the approximations mentioned above produce no appreciable effect for the resonance at 5.97 eV in $\text{Er}^{167}$ ($\Gamma_n:\Gamma_\gamma=1:3$). Deviations due to these approximations will occur for low neutron energies ($E\leq 5$ eV) and low atomic weights ($A\leq 50$).

Potential scattering and interference between resonant and potential scattering could not be neglected in the above calculations, however, as shown by Fig. 12. Therefore, the full cross-section expressions given by Eqs. (7) and (8) were used in the analysis.

Examples of the family of curves obtained by this analysis are shown in Fig. 13 for the resonances at 23.5 and 69.2 eV. In the latter case one has $\Gamma_n>\Gamma_\gamma$, and it is obvious that an accurate value cannot be obtained for $\Gamma_n$ but that $\Gamma_\gamma$ is well defined under these circumstances. To obtain the best values of the parameters and their uncertainties the following prescription was used: First, for each sample thickness the average capture area $C_{\text{obs}}$ was calculated as an average over all runs with this sample thickness. Then the uncertainty $\delta C_{\text{obs}}$ of this

---

[15] J. L. Friedes, Brookhaven National Laboratory Report BNL-8028, 1964 (unpublished).

mean value was estimated as described in Sec. V. The area curves ($\Gamma_n$ versus $\Gamma_\gamma$ curves) and their confidence bands were computed from $C_{\text{obs}}$, $C_{\text{obs}}+\delta C_{\text{obs}}$, and $C_{\text{obs}}-\delta C_{\text{obs}}$, respectively, and plotted (see Fig. 14). Now the confidence parameters $\sigma_i$ and $\tau_i$ ($i$ labels the different curves), as defined in Fig. 14, were read off, and also the partial widths $\Gamma_{\gamma,ij}\Gamma_{n,ij}$ at all intersections ($ij$ labels the intersection of the $i$th and $j$th curves). With the method of least squares one can show that the best values of the partial widths can be written in terms of the $\sigma_i$, $\tau_i$, $\Gamma_{\gamma,ij}$, and $\Gamma_{n,ij}$ as follows:

$$\Gamma_\gamma=\sum_{(ij)} w_{ij}\Gamma_{\gamma,ij}\Big/\sum_{(ij)} w_{ij},$$

$$\Gamma_n=\sum_{(ij)} w_{ij}\Gamma_{n,ij}\Big/\sum_{(ij)} w_{ij},\tag{23}$$

where

$$w_{ij}=(1/\tau_i\sigma_j-1/\sigma_i\tau_j)^2,\tag{24}$$

and where $\sum_{(ij)}\equiv\sum_i\sum_{j<i}$ represents simply a sum over all intersections. A straightforward application of the methods of error propagation in the least-squares formalism yields, for the uncertainties of the parameters,

$$\delta\Gamma_\gamma=\left(\sum_i\frac{1}{\sigma_i^2}\Big/\sum_{(ij)} w_{ij}\right)^{1/2},$$

$$\delta\Gamma_n=\left(\sum_i\frac{1}{\tau_i^2}\Big/\sum_{(ij)} w_{ij}\right)^{1/2}.\tag{25}$$

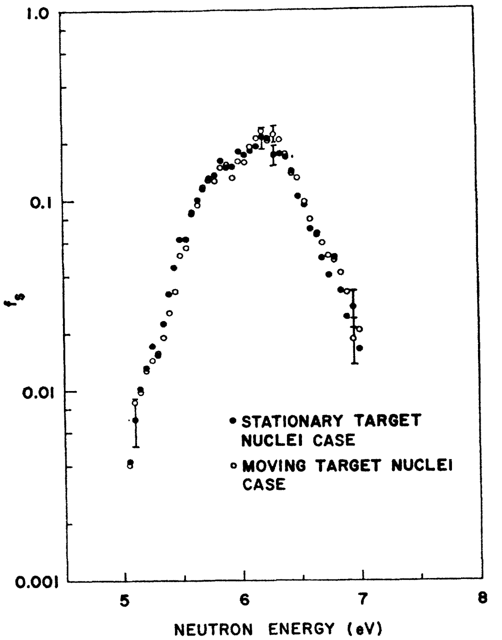

FIG. 11. Multiple-scattering contribution $f_s$ calculated with Monte Carlo codes for stationary target nuclei having Doppler-broadened cross sections (Ref. 9) and for moving target nuclei having unbroadened cross sections (Ref. 15). Input values were $E_0=5.97$ eV, $\Gamma_\gamma=70$ meV, $\Gamma_n=23.7$ meV, $g=\frac{1}{2}$, $R=8$ F, $A=167$, $n_{167}=1.858\times10^{21}$ nuclei/cm$^2$, and $T_{\text{eff}}=293$°K. Resulting capture area correction factors were $\mu=1.187$ for stationary-nuclei case and $\mu=1.191$ for moving-nuclei case. This figure shows that approximations made in Monte Carlo calculations (stationary target nuclei, infinite-slab geometry) do not lead to any appreciable error.

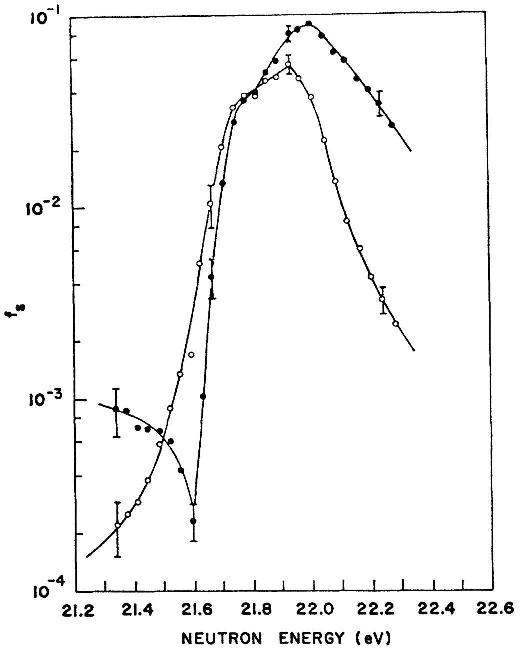

FIG. 12. Monte Carlo calculations showing importance of potential scattering: multiple-scattering contribution was calculated for $R=9.5$ F (solid circles) and $R=0$ (open circles). Parameters used were $E_0=21.8$ eV, $\Gamma_\gamma=21$ meV, $\Gamma_n=2.1$ meV, $g=1$, $A=232$, $n=3.88\times10^{-3}$ nuclei/barn, and $T_{\text{eff}}=300$°K.

Equations (23), (24), and (25) are rigorous for straight lines and sufficiently accurate for our purposes, since usually the area curves can be reasonably well approximated by straight lines in the region of interest, viz., near the point $(\Gamma_\gamma,\Gamma_n)$.

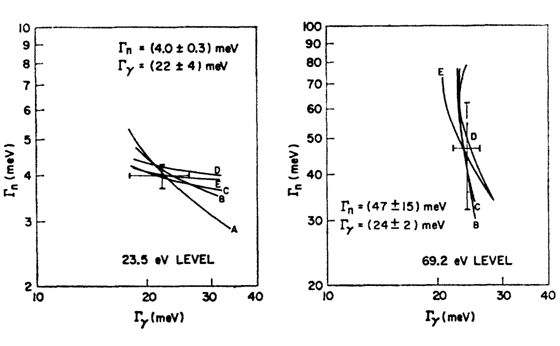

FIG. 13. Curves in $(\Gamma_\gamma,\Gamma_n)$ plane defined by experimental capture areas $C(n,E_1,E_2)$ from 23.5- and 69.2-eV resonances in thorium. Sample thicknesses are (in nuclei/b) $n_A=3.83\times10^{-3}$, $n_B=1.18\times10^{-3}$, $n_C=3.94\times10^{-4}$, $n_D=1.60\times10^{-4}$, and $n_E=3.52\times10^{-5}$.

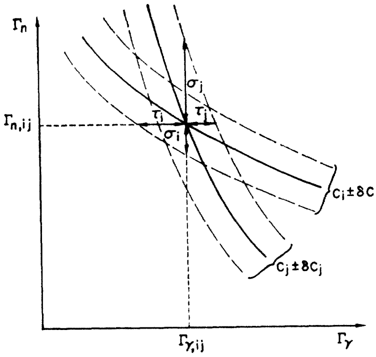

FIG. 14. Schematic representation of two area curves with their confidence bands near their intersection. This figure illustrates the quantities $\Gamma_{\gamma,ij}$, $\Gamma_{n,ij}$, $\sigma_i$, $\tau_i$ which occur in Eqs. (23)–(25).

## V. EXPERIMENTAL RESULTS

Table II gives the resonance parameters obtained for 11 $s$-wave levels in thorium for the neutron energy interval from 20 to 222 eV. The uncertainties in the parameters were calculated from the uncertainties assigned to the experimental capture areas $C(n,E_1,E_2)$ that define an intersection in the $(\Gamma_\gamma,\Gamma_n)$ plane, as described in the previous section. Table III lists the sources of error that contributed to the uncertainties in the experimental quantities $C(n,E_1,E_2)$.

TABLE II. Thorium resonance parameters.

| $E_0$(eV) | $\Gamma_n$(meV) | $\Gamma_\gamma$(meV) |
|---|---|---|
| 21.80±0.04 | 2.1± 0.2 | 21±5 |
| 23.47±0.04 | 4.0± 0.3 | 22±4 |
| 59.5 ±0.1 | 4.0± 0.4 | 22±7 |
| 69.2 ±0.1 | 47 ±15 | 24±2 |
| 113.1 ±0.2 | 14 ± 2 | 23±3 |
| 120.9 ±0.2 | 28 ± 8 | 24±3 |
| 129.3 ±0.2 | 3.7± 0.3 | ... |
| 170.7 ±0.3 | ... | 26±3 |
| 193.1 ±0.3 | 18 ± 3 | 24±4 |
| 199.8 ±0.3 | 10.6± 0.7 | ... |
| 221.9 ±0.4 | 33 ± 5 | 27±3 |

Several capture-area measurements of the same resonance were usually performed with a given sample thickness, so that the quantity $C(n,E_1,E_2)$ that defines a curve in the $(\Gamma_\gamma,\Gamma_n)$ plane was normally an average of the results of several independent measurements. Before the individual values of $C(n,E_1,E_2)$ were averaged they were first normalized to a given flight path $L_N$, flux exponent $\alpha_N$, and flux calibration constant $\epsilon_\gamma SK_N$, by

$$C_{Ni}(n,E_1,E_2)=C_i(n,E_1,E_2) \times(\epsilon SK_N/\epsilon SK_i)(L_N/L_i)(E_0{}^{\alpha_N-\alpha_i}). \quad (26)$$

This normalization procedure assumes that the quantity $C_i(n,E_1,E_2)/(\epsilon SK_iL_iE^{\alpha_i})$ is invariant to changes in experimental geometry, neutron flux intensity, and detector sensitivity. This assumption should be correct to first order if the boundaries of the area interval $(E_1,E_2)$ are wide enough to minimize resolution effects.

TABLE III. Uncertainty contributions to $\delta C/C$ from various sources of error.

| | $\delta C/C$ |
|---|---|
| 1. Counting statistics in $C(n,E_1,E_2)$. | 0.3 to 4% |
| 2. Counting statistics in $\epsilon_\gamma SK$ determination. | |
| 3. Background subtractions. | |
| 4. Boundaries $(E_1,E_2)$. | |
| 5. Beam monitor stability. | |
| 6. Gain stability. | |
| 7. Exponent $\alpha$ in flux energy dependence. | |
| 8. Flight path, $L$, determination. | ≤1% |
| 9. Dead-time corrections to observed counting rates. | |
| 10. Neighboring resonance contributions. | |
| 11. Resonant energy, $E_0$, determination. | |
| 12. Thickness (nuclei/cm$^2$) determination. | |
| 13. Sample area, $S$. | |
| 14. Presence of impurities in the samples. | |
| 15. Pulse pile-up effects. | |
| 16. Systematic uncertainty in $\epsilon_\gamma SK$. | 3% |
| 17. Uncertainty in assumption of constant efficiency, $\epsilon_\gamma$. | 3% |
| 18. Uncertainty in gamma-ray attenuation correction. | ≤0.5% |
| 19. Uncertainty in multiple scattering corrections (see Table IV). | ≤1.6% |

The deviations of the normalized areas from the average $(\bar{C}_N-C_{Ni})$ should then reflect the net uncertainty in $C_N(n,E_1,E_2)$ representative of items 1 through 7 in Table III, which shows the range of uncertainties calculated from the observed deviations for the levels under investigation.

The sources of error listed as items 8 through 15 were investigated and found to be negligible. Some of the more important measurements which were made to verify this conclusion are as follows. The effectiveness of the analyzer dead-time correction (item 9) was checked by measuring a capture area under various conditions of neutron beam intensity and comparing the corrected results. The agreement was excellent for the ranges of counting rates normally encountered in the course of a capture measurement.

In the computer code that generates the curve defined in the $(\Gamma_\gamma,\Gamma_n)$ plane by a capture area $C(n,E_1,E_2)$, only a maximum of seven neighboring resonances can be used in the cross-section calculations (item 10). The error introduced by using only the seven nearest-neighboring resonances was found to be negligible. In fact, the levels in thorium are, for the most part, well separated, and in many cases only a negligible error $(<0.3\%)$ would be introduced into the calculation by neglecting *all* neighboring resonances.

The effects of pulse pile-up on a capture area (item 15) were investigated by several procedures. One way, mentioned earlier, was to compare capture areas measured with a low beam intensity to those measured with a high beam intensity. Another check consisted of measuring a capture area with a 0.015-in.-thick thorium sample in the neutron beam and a 0.050-in.-thick thorium sample placed underneath the 0.015-in.-sample in such a way that it did not intercept the neutron beam. The radioactivity from both samples increased the ambient background by a factor of 3, yet no significant change was observed in the measured capture area. The same check was made using a 0.020-in. gold sample in place of the 0.015-in. thorium sample. In this case the background counting rates with and without the 0.050-in. thorium sample (outside the neutron beam but within the large liquid scintillator) differed by a factor of 20. Again, no significant change ($<1\%$) was observed in a given capture area (after background subtractions and dead-time corrections were made). A third check consisted of measuring pulse-height distributions from $Na^{24}$ sources of low and high activities and comparing the spectrum fraction, with a 4-MeV threshold as a function of counting rate. This test also confirmed that pulse pile-up effects were negligible at the counting rates normally used. Typical peak counting rates encountered while obtaining the thorium-capture data seldom exceeded $5\times10^4$ counts/sec. The peak counting rates presented to the time analyzer, with a 4-MeV bias, would be about one-half this figure, since $\epsilon_b \sim 0.5$ as seen in the right-hand side of Fig. 7.

The uncertainties assigned to a capture area because of items 16, 17, and 18 were discussed in Secs. IIIB, IIIC, and IIID. Item 17 applies only to levels other than the 21.8- and 23.5-eV levels. Item 18 applies only to samples with a thickness of $<0.015$ in.

The uncertainty assigned to a curve in the $(\Gamma_\gamma,\Gamma_n)$ plane because of the Monte Carlo nature of the calculation for multiple scattering events can be calculated by straightforward methods.[16] By taking a sufficiently large number of neutron histories in the calculations, this statistical error was kept small ($\leq 0.6\%$). A more significant source of error in the multiple scattering calculation is the uncertainty in the potential scattering cross section, $\sigma_p$. (Figure 12 illustrates the effect of resonant and potential-scattering interference on the secondary-capture probability $f_s$.) Reported values of $\sigma_p$ for thorium range from $(11.0\pm0.3)$ barns[17] to $(12.0\pm0.3)$ barns.[18] A value of $(11.4\pm10\%)$ barns for $\sigma_p$ was used in the calculations. The assigned uncertainty of 10% in $\sigma_p$ results in $\sim 4\%$ uncertainty to the calculated value of $C_s$. The "stationary nuclei" approximation contributes another uncertainty of $\sim 2\%$ to $C_s$. Table IV presents the results of the multiple scattering calculation for the two resonances (69.2 and 129.3 eV) which gave the largest and smallest ratio $C_s/C$, respectively. The net uncertainties in $C_s/C$ for these cases are also presented in Table IV.

The question of how accurately the mathematical model in the computer program reproduces the physical processes in the capture sample is not easily answered in a quantitative manner. The theoretical basis of the scattering processes in the eV energy region is certainly sound. The effects of approximations employed in the calculations are also easily evaluated in most cases. However, the best evidence that a computer code does what it is supposed to do is to compare calculated results with experimental results, preferably in extreme cases. For this purpose, calculations were performed of the resonance shape for the 18.8-eV level in $W^{186}$, where $\Gamma_n/\Gamma_\gamma \approx 6$.[19] The results were normalized to the peak of the experimentally observed shape of the resonance in Fig. 15. For this case the calculated value for $C_s/C$ is $0.67\pm0.03$, which means that on the average two out of

TABLE IV. Fraction of capture area ($C_s/C$) resulting from multiple scattering events in the sample, for the levels investigated that had the largest and smallest effects.

| $E_0$ (eV) | Sample thickness (in.) | $C_s/C$ | $\delta C_s/C$ |
|---|---|---|---|
| 69.2 | 0.050 | 0.35 | 0.016 |
| | 0.015 | 0.26 | 0.013 |
| | 0.005 | 0.17 | 0.008 |
| | 0.002 | 0.09 | 0.004 |
| | 0.0005 | 0.03 | $\sim 0$ |
| 129.3 | 0.050 | 0.06 | 0.003 |
| | 0.015 | 0.02 | $\sim 0$ |
| | 0.005 | 0.009 | $\sim 0$ |
| | 0.002 | 0.005 | $\sim 0$ |

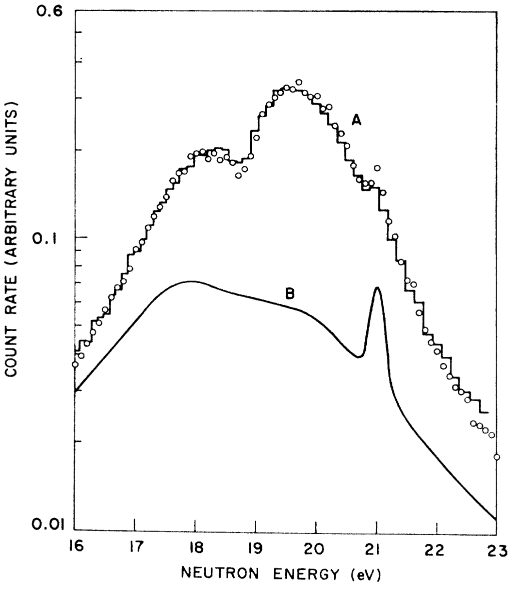

FIG. 15. Comparison of calculated (open circles) and experimental (histogram) counting rate [curve A in $WO_2$ sample enriched with $W^{186}$ (97.2% abundance)]. Sample thickness was 0.011 atom/b. Curve B represents calculated counting rate for first interactions of incident neutron beam, relative to curve A. Calculations include presence of $W^{182}$ (1% abundance), which accounts for weak level at 21 eV.

---

[16] H. Kahn, U. S. Atomic Energy Commission Report AECU-3259, 1956 (unpublished).

[17] J. E. Evans (Comp.), European-American Nuclear Data Committee Report EANDC/UK/-21 "U", p. 26, 1963 (unpublished).

[18] K. K. Seth *et al.*, Phys. Rev. **110**, 692 (1958).

[19] A. B. Smith (Comp.), European-American Nuclear Data Committee Report EANDC(US)-57 "U", 1964, p. 69 (unpublished).

three captured neutrons have previously been scattered. That this is an extreme case is also illustrated by the drastic departure from the Breit-Wigner shape (curve B in Fig. 15) that is observed in the calculated and experimental shapes (curve A in Fig. 15). The good agreement between the gross features of the calculated and observed shapes is good evidence that the mathematical model is adequate.

## VI. DISCUSSION

The radiation widths given in Table II are in quite good agreement with recent results from Harwell[20] and Saclay.[21] There is also fair agreement with recent values measured by the Columbia[3] group in those cases where the measurements overlap. The average value of $\Gamma_\gamma$, obtained from a weighted average of the data appearing in Table II, is 24.5±1.5 meV. This value is in disagreement with the previously favored value[1] for $\Gamma_\gamma$ of 34±7 meV.

A check on the validity of the results reported here was made by calculating the thorium infinite dilution resonance integral, defined by

$$I_\infty = \int_{0.5\text{ eV}}^{\infty} \sigma_\gamma \frac{dE}{E},$$

and comparing the result with integral measurements. This calculation gave a value for $I_\infty$ of 84.5±4.5 b, which is in good agreement with the measured integral value of 83±3 b. The measured integral value represents a weighted average of several measurements.[22–24] The various energy regions contributed to $I_\infty$ as follows: 1.0 b for the region from 0.5 to 19 eV, 80.8 b for the region from 19 eV to 4 keV, and 2.7 b for the energy region above 4 keV. In the evaluation of this integral the parameters reported in Table II were used up to 222 eV. In the energy region from 222 to 4000 eV Columbia neutron widths were used, along with a $\Gamma_\gamma$ of 24.5 meV. Above 4000 eV a statistical calculation employing average resonance parameters was used for the *s*- and *p*-wave contributions.[25]

Resonance parameters have been obtained for the predominant *s*-wave resonances that occur in the neutron energy region from 20 to 222 eV. These levels account for approximately 85% of the thorium infinite-dilution resonance integral. The results indicate that, within the errors given in Table II, the radiation width is a constant for the levels investigated. The parameters reported in this paper were obtained from multiple-sample capture measurements alone. Specifically, $\sigma(n,\gamma)$ measurements are best suited for obtaining $\Gamma_\gamma$ values when $\Gamma_n \geq \Gamma_\gamma$ and for obtaining $\Gamma_n$ values when $\Gamma_n \ll \Gamma_\gamma$.

## ACKNOWLEDGMENTS

We are grateful to J. R. Beyster for his encouragement and many helpful discussions throughout the course of the work, to the General Atomic linear accelerator operating staff for their help with the beam, to M. K. Drake and J. D. Garrison for their assistance in the resonance integral calculations, and to D. L. Huffman for aid in data reduction.

We would also like to thank J. H. Gibbons of Oak Ridge National Laboratory, H. Palevsky of Brookhaven National Laboratory, E. R. Rae of Harwell, and L. W. Nordheim of General Atomic for helpful suggestions concerning this work.

---

[20] E. R. Rae (private communication).

[21] R. Joly and P. Ribon (private communication).

[22] M. Brose, Nucl. Sci. Eng. **19**, 244 (1964).

[23] W. K. Foell and T. J. Connolly, Nucl. Sci. Eng. **21**, 406 (1965).

[24] René Vidal, Commissariat à l'Energie Atomique Report CEA-R-2486, 1964 (unpublished).

[25] L. W. Nordheim, General Atomic Report GA-3973, 1963 (unpublished).